Electrostatics for Exploring the Nature of the Hydrogen Bonding in Polyethylene Oxide Hydration

Yosslen Aray,*,†,‡ Manuel Marquez,†,§,||,⊥ Jesus Rodríguez,† David Vega,# Yamil Simón-Manso,‡ Santiago Coll,† Carlos Gonzalez,‡ and David A. Weitz||

Centro de Quimica, IVIC, Apartado 21827, Caracas 1020 A, Venezuela, Physical and Chemical Properties Division, National Institute of Standards and Technologies, NIST, Gaithersburg, Maryland 20899, The Nanotechnology Laboratory, Kraft Foods R&D, 801 Waukegan Road, Glenview, Illinois 60025, Department of Physics and DEAS, Harvard University, 29 Oxford Street, Cambridge, Massachusetts 02138, Los Alamos National Laboratory, Chemistry Division, Los Alamos, New Mexico 87545, and FACYT, Universidad de Carabobo, Valencia, Venezuela

Received: September 30, 2003; In Final Form: December 2, 2003

Binding between water and models of poly(ethylene oxide), $(CH_2-CH_2-O)_n$, $n = 2-40$, has been studied using the topographic features of the electrostatic potential, $V(\mathbf{r})$, and standard density functional theory methods. It was found that, in general, the contour around the minima of the oxygen atoms overlap forming a negative-valued spiral coiled around a positive-valued helix. The positive zone defines a helical groove in the O−C−C−O units where minima lone pairs critical points are located. Topological analysis of the water molecule has also suggested that the attractive electrostatic effect between the positive water O−H zone and the negative PEO lone pairs plays an important role in the hydrogen bonding of the PEO−water system. Thus, the $V(\mathbf{r})$ topology predicts a coil of water molecules around the PEO chain forming hydrogen bonding with two sites of ether oxygens. This coil is formed in such a way that more water molecules accumulate on the cavities surrounding the poly(ethylene oxide)'s oxygen atoms where the minima of the negative zone are located.

Introduction

Poly(ethylene oxide) (PEO) is a nonionic surfactant of great scientific and technological interest for a wide variety of applications, many of which depend on the properties of the polymer in aqueous solution.[1] It is commonly used as lubricants, dispersants, plasticizers, and recovery agents of tertiary oils and as friction reducers in the flow of water trough ducts and channels.[2−6] PEO gels and other aggregates of PEO are also good candidates for drug delivery purposes. [7−10] More recently, researchers have focused their attention on the use of PEO in biomedical applications. [11] Given that PEO is generally biocompatible it has been suggested as a viable replacement for a variety of biopolymers providing important information related to their behavior and function. Additionally, PEO is a very important part of the so-called "shake gels" (SG). "Shake gels"[12] are formed by aqueous solutions of synthetic clays and polymers that form a gel after the solution is shaken. The most common SG is built from mixtures of Laponite, poly(ethylene oxide), and water. These materials form a clear solution that leads to a gel once shaken. This gel relaxes back to a liquid after a certain period of time that depends on the Laponite and PEO concentrations. At longer times, the mixture forms a permanent gel due to an aging process that is not well understood. Despite the considerable interest in the properties of these materials, the design and synthesis of SGs has relied on an empirical approach that entails long and expensive trial-and-error experimental procedures. Fundamental questions dealing with the nature of the interactions between the components that lead to gel formation after shaking need to be answered in order to pave the way for the rational design of these materials. Simulations of these systems based on reliable theoretical methodologies offer a powerful tool that can complement the experimental data in order to shed some light on the mechanisms governing the formation and stability of "shake gels". Water−PEO−Laponite is a complicated system that entails a competition between the PEO and water binding to the clay. To understand the net effects of these interactions in the actual system, it is useful to understand each individual one. As part of an ongoing systematic study dealing with the nature of these interactions, we recently performed quantum chemical calculations in order to assess the role played by the electrostatics in the binding between the Laponite surface and water.[13] In this work we present the results of theoretical calculations on the water−PEO system making use of the topographic features of the molecular electrostatic potential, $V(\mathbf{r})$, which are particularly useful for understanding the hydration process.[14−18]

A large amount of experimental and theoretical studies of the water−PEO system have been reported in the literature[2,19−26]. A general conclusion arising from these studies is that hydrogen bonding plays an important role in the interaction between PEO and water. PEO is characterized by a sequence of monomers, which in water can adopt the local conformations (O−C−C−O dihedral sequences) tgt, tgg, tg^+g^-, ttt, etc. (with t = trans, and g = gauche). The same studies[19−26] indicate that the tgt and tgg conformers are favored under low concentration and low temperature conditions. These two conformers exhibit a substantial hydrophilic character while the rest are essentially

* Corresponding author. Fax: (+58) 212 504 1350. E-mail: yaray@ivic.ve.
† Centro de Quimica, IVIC.
‡ National Institute of Standards and Technologies, NIST.
§ Kraft Foods R&D.
|| Harvard University.
⊥ Los Alamos National Laboratory.
Universidad de Carabobo.

10.1021/jp036921o CCC: $27.50
Published on Web 01/24/2004

hydrophobic. The population of the hydrophobic conformers increases with concentration and temperature. A similar trend was obtained for the average fraction of hydrogen bonding between PEO and water, PEO−W, and between water and water, W−W, using a mean field-like[24] approach and a molecular dynamics simulation.[22] The fraction of these hydrogen bonds was found to be rather large at low temperatures and concentrations. On most systems, the most stable conformation (cis, trans, and/or gauche) is the result of the combination of different factors such as steric repulsions, trans effect, hyperconjugation, hydrogen bonding, and solvent effects.[27] However, given the previous evidences, it would appear that in these systems, hydrogen bond plays an important role in the conformational preference.

In general, hydrogen bonds are the results of a delicate balance between electrostatic interactions, exchange and dispersion forces. In this study, we just focus on the electrostatic component of these interactions. To achieve this goal, we have carried out a systematic analysis of the topology of $V(\mathbf{r})$ for PEO chains $(CH_2-CH_2-O)_n$, $n = 2-40$, using standard density functional theory, DFT, methods. This methodology is particularly useful for studying the system at low temperatures, which favor hydrophilic conformations. From the outset, it should be pointed out that the study discussed in this work focuses only on the electrostatics of this system computed under ideal conditions (zero temperature and low concentrations), and that no attempt is made to extrapolate these results to explain dynamics and entropic effects that might be important factors in the interaction between PEO and water. To our knowledge, this is the first systematic theoretical study of the electrostatics of this system using density functional theory. Ample evidence in the literature indicates that the current DFT functionals tend to underestimate the binding in hydrogen-bonded systems when compared to highly correlated ab initio molecular orbital theory.[28] The size of the species in this work make the use of correlated ab initio computations a daunting task. Given that our final goal is the study of the significantly larger Laponite−PEO−water system, where the use of such methods is almost impossible, it is clear that DFT offers the best balance between reliability and computational efficiency.

$V(\mathbf{r})$ at a point $\boldsymbol{r}$ generated by a molecule is given by[16]

$$V(\mathbf{r}) = V_N(\mathbf{r}) + V_E(\mathbf{r}) = \sum_a Z_a / |\mathbf{r} - R_a|^{-1} + \int \rho(\mathbf{r}')|\mathbf{r} - \mathbf{r}'|^{-1} \mathrm{d}\mathbf{r}' \quad (1)$$

where the two terms represent the bare nuclear and electronic contributions, respectively, to the total electrostatic potential. The sign of $V(\mathbf{r})$ at a given point represents whether the nuclear or electronic effects are dominant. The topological properties of $V(\mathbf{r})$ are summarized by its critical points, CP. These are points where the gradient vector field, $\nabla V(\mathbf{r})$ vanishes, and they are classified by the $V(\mathbf{r})$ curvatures or three eigenvalues λ_i ($i = 1$, 2, and 3) of the corresponding Hessian matrix ($\mathbf{H}_{ij} = \partial^2 V(\mathbf{r})/\partial x_i\, \partial x_j$). In molecules and crystals, there are four types of these extremes that are labeled by their rank (number of nonzero eigenvalues) and signatures (excess number of positive over negative eigenvalues). These can be maxima (3, −3), minima (3, +3), or (3, −1) and (3, +1) saddles that bridge either two minima or two maxima. For the region nearest to the nucleus, V_N dominates and $V(\mathbf{r})$ has exactly the same topology of the electron density, $\rho(\mathbf{r})$,[29] i.e., positive-valued maxima at the nuclear site and a positive-valued (3, −1) bond saddle between every pair of bonded atoms. For the region where V_E dominates, $(V(\mathbf{r}) < 0)$ the $V(\mathbf{r})$ topography can be more complex. However, it is well-known that lone pairs of electrons as well as double π bonds (C═C, C═N, etc.) are generally characterized as negative valued (3, +3) minima.[17,18] The set of CPs of a molecule are unique and hence their existence and nature offer a signature of the structure of the molecule. The main topographic features of $V(\mathbf{r})$ are easily visualized using three-dimensional (3D) maps of isovalued contours. In these maps, the minima show their distinctive topological features: equipotential contours that becomes more and more close to the minimum as the absolute magnitude of the isosurface value is increased toward the $V(\mathbf{r})$ value at the minimum. Figure 1 shows the $V(\mathbf{r})$ topological features of an isolated water molecule, the negative potential (blue, yellow, and green iso-surfaces) is located over the nonbonding region of the oxygen atom forming a lone pair pattern like a "rabbit ears" with two negative-valued minima (red spheres) connected by a (3, +1) saddle point. The $V(\mathbf{r})$ over the entire nuclear region is positive (brown zone) with a saddle CP associated to each OH bond. By locating CPs in substrate electrostatic potentials, one can precisely identify the host sites in which water molecules should bind. Maintaining complementary between the $V(\mathbf{r})$ features of substrate and water, the positive valued $V(\mathbf{r})$ zone of the hydrogen atoms in the water molecules are positioned over the minima of the negative $V(\mathbf{r})$ zone of the substrate.[17,18] Additionally, the $V(\mathbf{r})$ topology-based theory predicts that the attractive interactions $(OH)_{water} \rightarrow (\text{negative minima})_{substrate}$ will be stronger as the absolute value of $V(\mathbf{r})$ at the minima increases.[13,17,18]

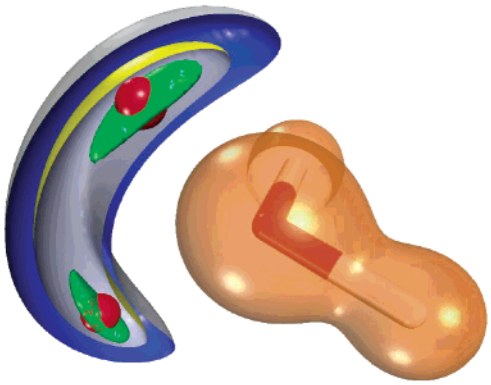

Figure 1. 3D-contour maps of $V(\mathbf{r})$ for the isolate H_2O molecule. Brown contour denotes the positive zone. Blue, yellow, and green iso-surfaces denote negative zone with values of −78.78, 105.04, and 105.04 kJ/mol, respectively. Red spheres denote the minima critical points ($V(\mathbf{r}) = -170.69$ kJ/mol) characterizing the oxygen lone pairs. Red and white cylinders denote the oxygen and hydrogen atoms.

The potential $V(\mathbf{r})$ was calculated by means of the DMol[3] [30,31] program using the Kohn-Sham Hamiltonian with the gradient-corrected Perdew-Becke-Ernzerhof (PBE) exchange-correlation functional[32] and a novel and efficient algorithm for the systematic determination of all critical points in $V(\mathbf{r})$. Details of this algorithm and its implementation will be published in an incoming manuscript**.** DMol[3] calculates variational self-consistent solutions to the DFT equations, expressed in a numerical atomic orbital basis. The solutions to these equations provide the molecular electron densities, which can be used to evaluate the total electrostatic potential of the system. The numerical double-ζ plus polarization basis set DNP[31] was used in all calculations.

The topology of $V(\mathbf{r})$ was analyzed using an algorithm developed in our laboratory, similar to those developed for the study of the electronic density topology.[33−34] The CPs were calculated using the Newton−Raphson (NR) technique.[35] The

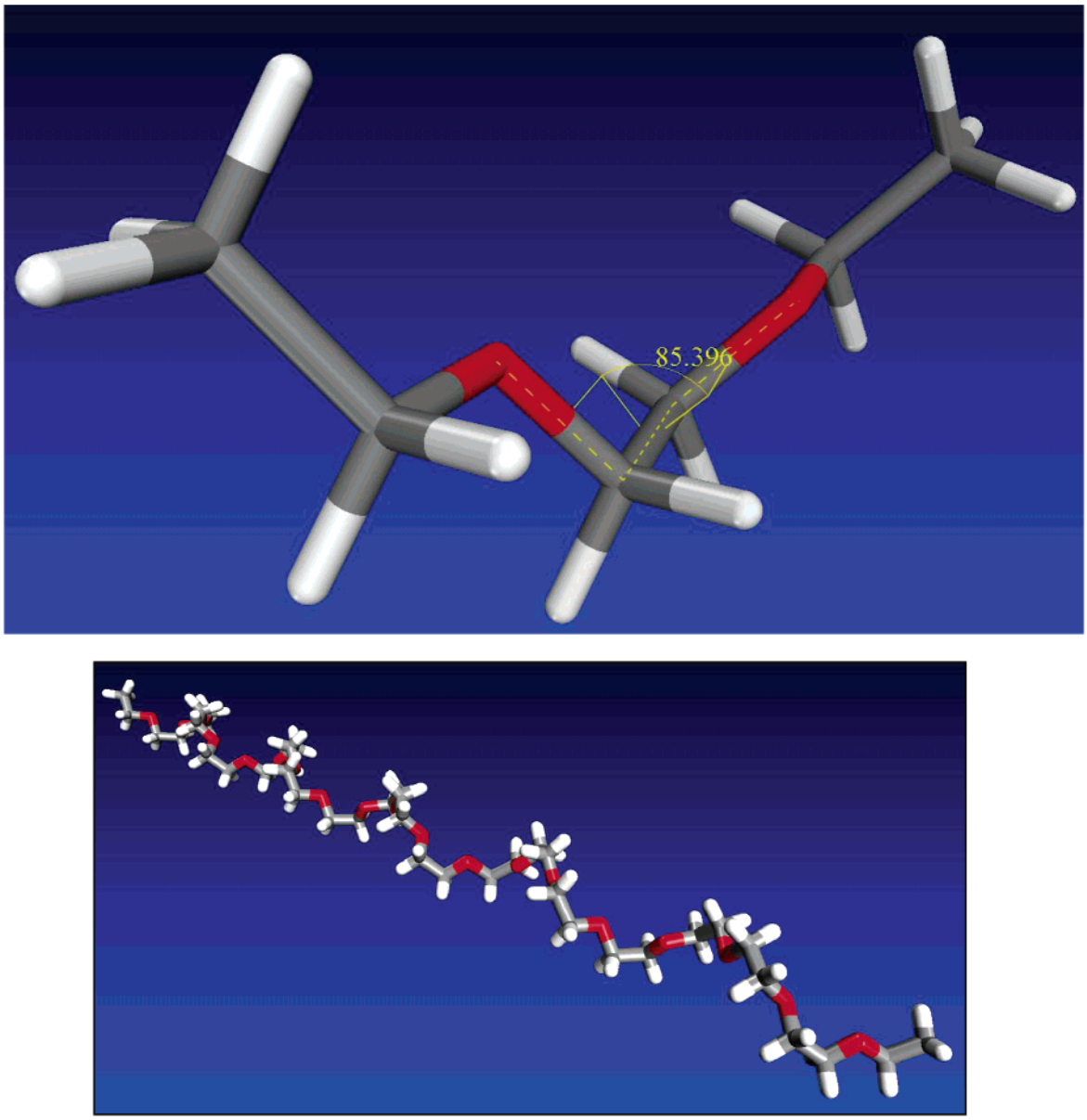

Figure 2. Cylinder models of (top) PEO2 and (bottom) PEO20. Red, gray, and white cylinders denote the oxygen, carbon, and hydrogen atoms, respectively. In top is shown the O−C−C−O dihedral angle (85.4 degrees) that characterizes the tgt PEO2 conformation.

algorithm starts from a truncated Taylor expansion at a point $\mathbf{r} = \mathbf{r}_0 + \mathbf{h}$, about $\boldsymbol{r}_0$ of a multidimensional scalar function ($\nabla V(\boldsymbol{r})$):

$$\nabla V(\mathbf{r}) = \nabla V(\mathbf{r}_0) + \mathbf{H}_0\mathbf{h} + \text{higher order terms} \qquad (2)$$

where **H** is the Hessian (the Jacobian of $\nabla V(\mathbf{r})$) at point $\boldsymbol{r}_0$. Given that a CP is characterized by $\nabla V(\boldsymbol{r}) = 0$, the optimal step $\mathbf{h}^*$ is then given by $\mathbf{h}^* = -\mathbf{H}^{-1}\nabla V(\mathbf{r}_0)$. This second-order correction is then used to obtain a vector $\mathbf{r}_{new} = \mathbf{r}_{old} + t\mathbf{h}^*$ (t is a small value) and the process is iterated to $\nabla V(\boldsymbol{r}) = 0$. The NR algorithm requires the evaluation of the first V′ and second V″ partial derivatives of $V(\boldsymbol{r})$, at arbitrary points $\boldsymbol{r}$. These partial derivatives are evaluated using a five-degree Lagrange polynomial interpolation of $V(\boldsymbol{r})$ and are fed into an automated algorithm for the systematic determination of the all molecule CPs.

Results

The geometry of several isolated PEO chains $(CH_2-CH_2-O)_n$, $n = 2-40$, were fully optimized at the DFT level. In this work we adopt the notation PEO*n* with $n = 2-40$ to indicate the number of monomers considered in the chain. For all of the chains an all-tgt extended conformation, i.e., a complete sequence of tgt conformers, with an average O−C−C−O dihedral angle of 86 degrees, was found to be the global minima. Figure 2 shows a cylinder model of the optimized geometry for PEO2 and PEO20 and Figures 3 and 4 show the main topological characteristics of the electrostatic potential for these chains of monomers. For each oxygen atom, a pair of nonbonded minima (red spheres) connected by a saddle (3, +1) CP at the negative zone (blue) was found. As expected, $V(\boldsymbol{r})$ is positive (light brown zone) over the entire nuclear region with a (3, −1) CP for each bond in this zone. In general, the contour around the minima of the O atoms overlap, forming a negative-valued spiral (blue zone) coiled around a positive-valued helix (light brown zone). The positive zone defines a helical groove in the O−C−C−O units where the lone pairs are located. It was found that the calculated values of the topological properties that characterize these CPs are almost unaffected by the length of the model. Table 1 lists these values just for a monomer. This

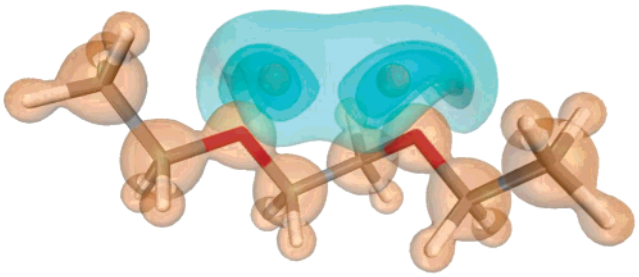

Figure 3. $V(\mathbf{r})$ contours map of PEO2. Blue and brown contours denote the negative and positive valued zones of the potential. Red spheres denote the minima CPs characterizing the oxygen lone pairs.

table also includes the corresponding values for an isolated water molecule. Note that the $V(\mathbf{r})$ values of the minima of the oxygen lone pairs in PEO monomers are more negative than the ones corresponding to the water molecule. In addition, the positive value at the O−H bond in water is 50% bigger than the corresponding value of the C−H in the monomers. These facts suggest that the attractive electrostatic interaction between the positive water O−H bond and the negative PEO lone pairs is the driving force for the hydrogen bonding on PEO−water. Thus, the $V(\mathbf{r})$ topology predicts (see Figure 4) a coil (the negative blue zone is the hydrophilic region) of water molecules around the PEO chain forming hydrogen bonding with two sites of ether oxygens. This coil is formed in such a way that more

TABLE 1: Topological Properties of the Electrostatic Potential at the Critical Points, $V(\mathbf{r}_c)$, for the Monomer of the Studied PEO Models, for an Isolated Water Molecule, and for a Water Molecule Adsorbed on the O−C−C−O Cavity

CP	λ_1 (au)	λ_2 (au)	λ_3 (au)	$V(\mathbf{r}_c)$ (kJ/mol)
		$-CH_2CH_2O-$		
Two minima by oxygen atom	0.0079	0.0313	0.11039	−194.8514
(3, −1) C−C bonds	−1.0449	−0.9977	4.9461	1649.9346
(3, −1) C−O bonds	−1.8393	−1.7129	7.3528	2272.0411
(3, −1) C−H bonds	−2.1735	−2.1113	7.5583	2025.1943
		H_2O		
Two minima at the oxygen atom	0.0017	0.0383	0.1900	−170.6920
Two (3, 1) OH bond	−4.387	−4.180	13.259	3010.4807
		H_2O Adsorbed on a O−C−C−O Pocket of PEO4		
Minima at the H_2O oxygen atom	0.0084	0.0326	0.1586	−289.3885
(3, −1) OH bond	−4.4831	−4.1954	13.2118	2794.0959

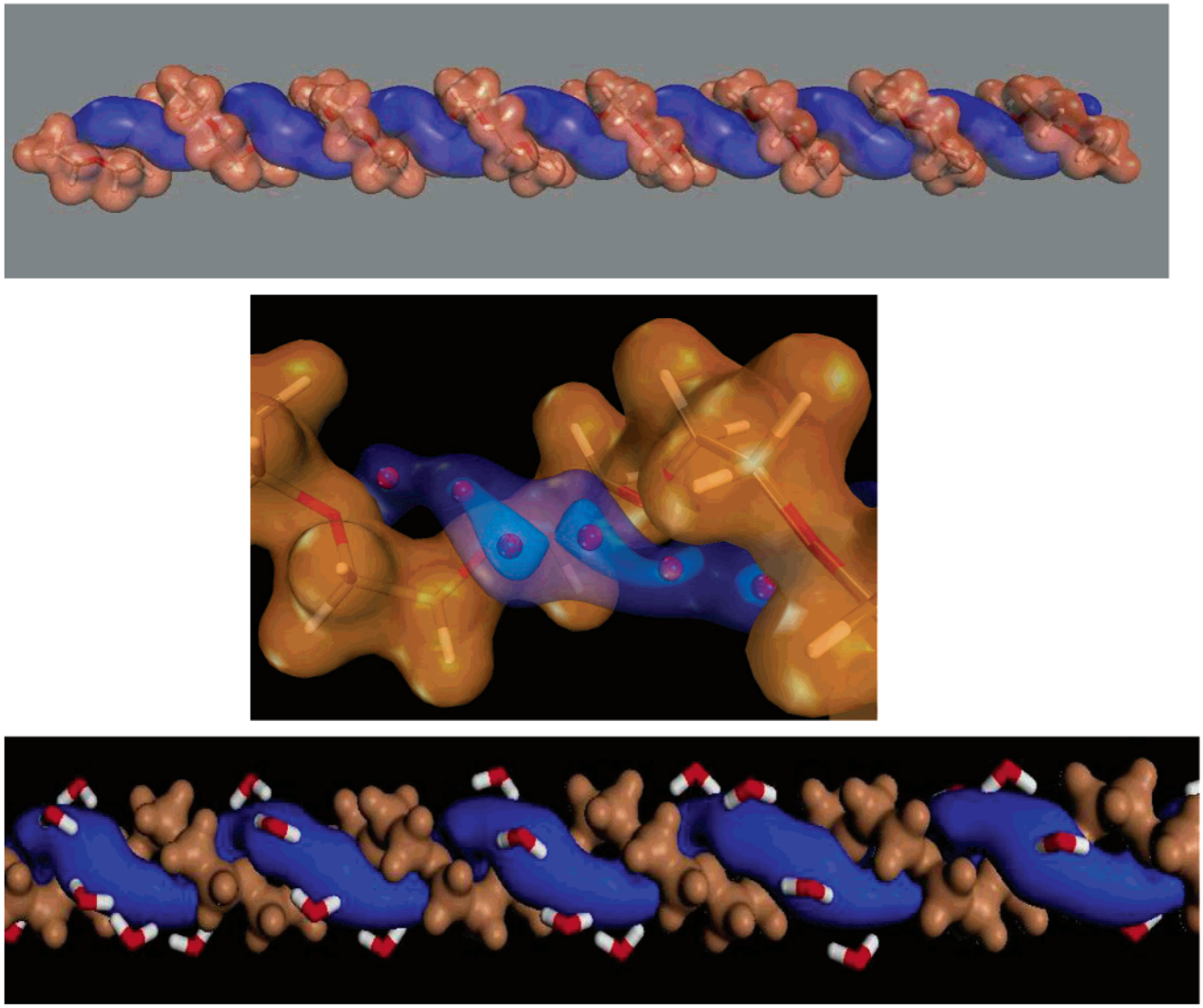

Figure 4. (Top) $V(\mathbf{r})$ contours map of PEO20. Blue and brown contours denote the negative and positive valued zones of the potential. (Middle) Details of a section of the polymer showing the characteristic network of blue contours around the minima (red spheres) CPs of the oxygen atoms. (Bottom) $V(\mathbf{r})$ topology predicts a coil of water molecules hydrogen-bonded around the polymer.

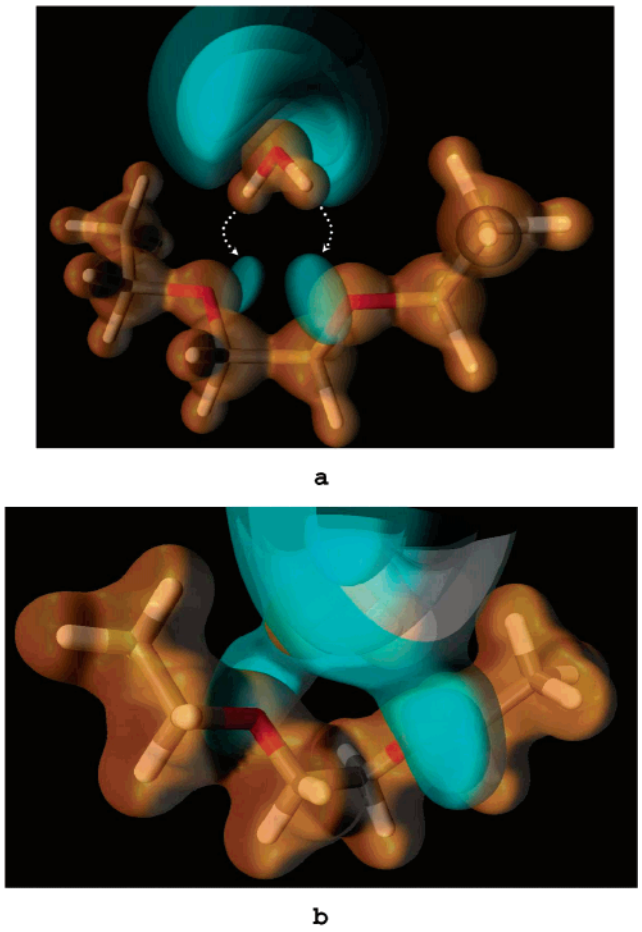

Figure 5. A H_2O molecule adsorbed on PEO2 describing two H−O hydrogen bond frameworks. (a) Initial configuration, (b) Optimized geometry. Blue and brown contours denote the negative and positive valued $V(\mathbf{r})$ zones. White arrows in (a) show the attractive interactions $(OH)_{water} \rightarrow (\text{negative minima})_{PEO2}$

water molecules accumulate on the cavities surrounding the PEO's oxygen atoms where the minima of the negative zone are located.

To test the validity of the prediction made by the $V(\mathbf{r})$ topology, the binding of water to PEO2, PEO4, and PEO20 was explicitly explored by performing full geometry optimizations in internal coordinates using the DMol[3] program. In the case of PEO2, the $V(\mathbf{r})$ topology model previously discussed predicts the binding of one molecule in such a way that each OH bond is aligned with the lone pair corresponding to the adjacent ether oxygens of the polymer (Figure 5a). Full geometry optimization of the H_2O−PEO2 system confirms such prediction. The electrostatic potential contour map for the optimized geometry is shown in Figure (5b). The negative area (blue in Figure 5b) of the potential contains the water molecule. This area fills the space determined by the O−C−C−O unit complementing the positive area (brown in Figure 5b) that covers the entire nuclear region of PEO2. The computed binding energy (BE) of water on PEO2 is 34.06 kJ/mol, in excellent agreement the value of 37.62 kJ/mol previously reported using MP2 at the D95** level.[26] Our computed BE value is 11.72 kJ/mol larger than corresponding binding energy of water dimer computed at the same level of theory (22.35 kJ/mol). Despite the success of the $V(\mathbf{r})$ model in predicting the binding mechanism between one water molecule and the PEO2 molecule, it is clear that this system does not include the possible electrostatic interactions between the water molecules that can

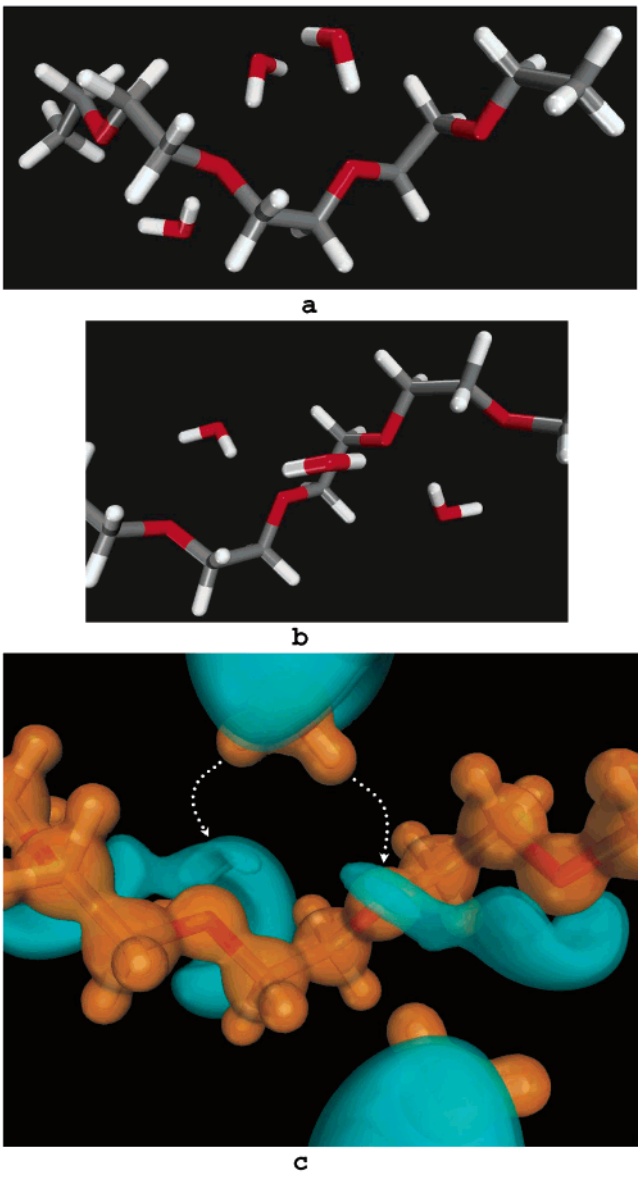

Figure 6. (a) and (b) show two different conformations of three water molecules adsorbed on PEO4. In (a) the water molecules at the top are doing a bridge between them. (c) Contours map of $V(\mathbf{r})$ for the initial geometry of 4b. Blue contours denote the negative valued zone of the potential. White arrows in (c) show the attractive interaction of the water OH positive zone toward two minima located at neighbor oxygen atoms on PEO4.

be important in the real solvated system. To test for the ability of the model to properly describe these interactions, we have applied it to a case where three molecules of water bind to the PEO4 system. According to the $V(\mathbf{r})$ topology, most of the water arrangements around the polymer are mainly dominated by the interactions shown in Figure 6. In one case (Figure 6a), a water molecule forms a hydrogen bond with an ether's oxygen on the polymer and another hydrogen bond with an adjacent water molecule. A second kind of interaction, similar to the H_2O−PEO2 case is shown in Figure 6b, where each H_2O molecule is located on each O−C−C−O tgt local site forming two hydrogen bonds with the minima lone pairs of the ether oxygens. To predict which of the two structures showed in Figure 6 should be more stable, we have calculated the topological properties of $V(\mathbf{r})$ for just a H_2O molecule adsorbed on PEO4 making only one hydrogen bond in the water−PEO system. The results listed in Table 1 indicate that the value of the potential at the minima

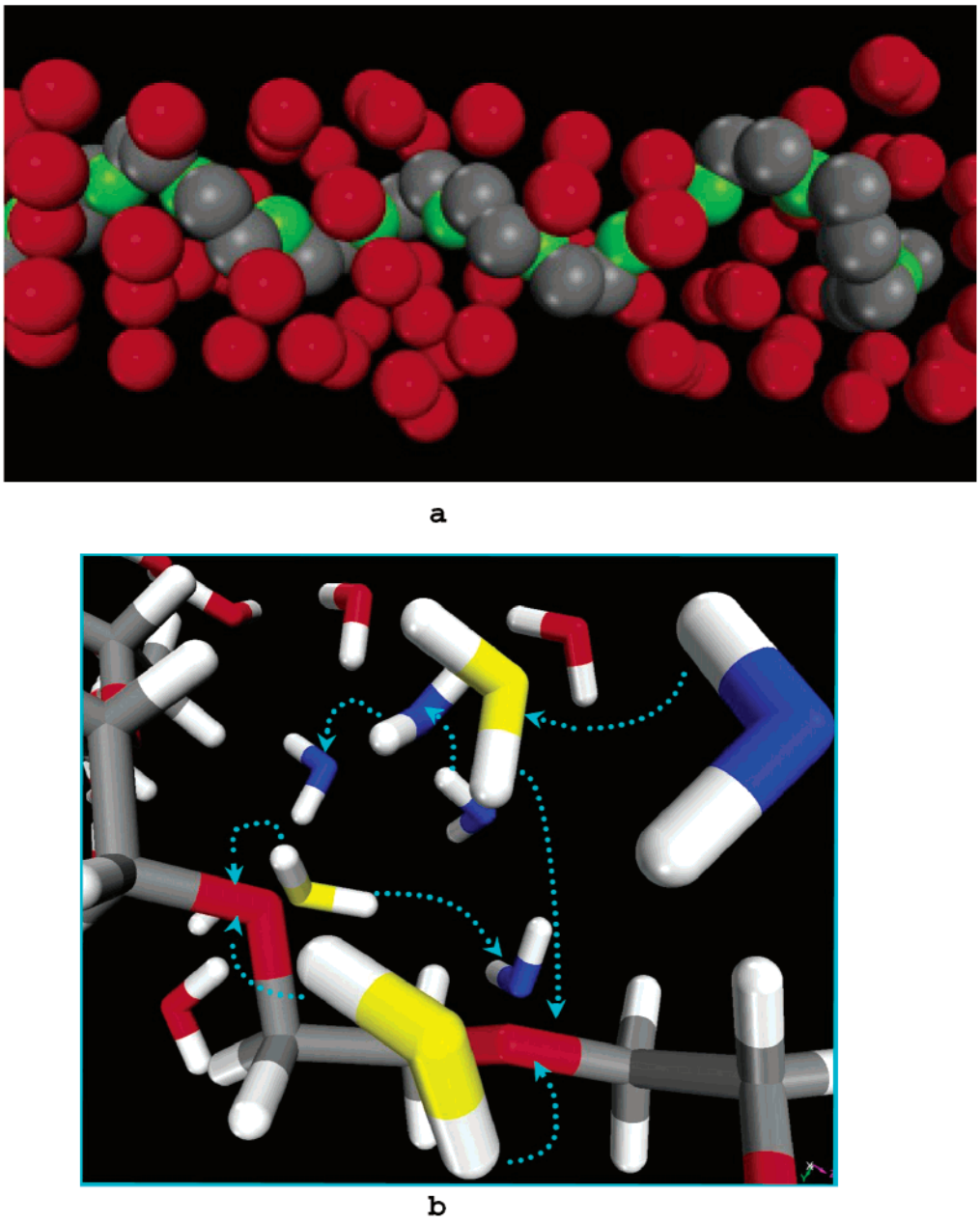

Figure 7. (a) A CPK model of a section of 118 water molecules adsorbed on PEO20. For a better visualization the hydrogen atoms have been removed. Red, green, and gray spheres denote the water oxygen, ether oxygen, and carbon atoms of the polymer, respectively. (b) A detail view of the water molecules around an O−C−C−O unit. Yellow and blue cylinders denote oxygen of the first and second layers of water, respectively. Blue lines denote the hydrogen H−O bonds.

lone pairs of the adsorbed H_2O molecule is 100% deeper than the corresponding value for the oxygen atoms of PEO4. On the basis of these results, one should expect a larger binding energy for the adsorption processes involving the kinds of interactions displayed in Figure 4a, where adjacent adsorbed water molecules form a hydrogen bond between them. As with the H_2O−PEO2 case, we have performed full geometry optimizations and corresponding BEs of the H_2O−PEO4 systems in order to test the predictions of the V(***r***) model. The computed BE indicate that the conformation of Figure 6a (total energy = −924.535176 au) is 6.95 kJ/mol more stable than the one in Figure 6b (total energy = −924.532520 au) corroborating the $V(\boldsymbol{r})$ topologic prediction. Figure 6c shows the topologic maps of the initial geometry corresponding to the case considered in Figure 6a.

Topological analysis of all the cases that we have studied, showed that bonding of the first layer of water molecules on PEO leads to an appreciable increment of the absolute value at the adsorbed water oxygen minima lone pairs favoring the formation of a second layer of water molecules attached on the first one. Using the *Amorphous Cell* program[36] we have randomly adjusted 118 molecules of water around a PEO20 inside a box of dimensions 10.2 × 10.2 × 56.2 Å, which it is enough to accommodate two solvation shells of water around the polymer. The geometry was fully optimized using the DMol[3] program with the density functional Semi-core Pseudopotential approach.[37] It was observed (Figure 7a) that the water molecules concentrate inside the O−C−C−O core interstitial region neighboring the PEO oxygen atoms and that they are depleted around the carbon atoms (gray spheres in Figure 7a). Figure 7b shows in detail the pattern of OH bonds surrounding the O−C−C−O area. As the figure indicates, the deepest negative zone of $V(\boldsymbol{r})$ which is located in the O−C−C−O units creates a "pocket" that promotes the water clustering around the water molecules directly bonded to the PEO. As predicted by the $V(\boldsymbol{r})$

topology, PEO−water interactions exhibit two different types of hydrogen bonds: O_{ether}−water−O_{ether} and O_{ether}−water−water−O_{ether}. The all-tgt extended conformation is still conserved in the solvated PEO20. This result is in excellent agreement with a molecular dynamics simulation that reports an increase in the tgt population with a decrease in temperature.[23] For low concentrated solution of PEO this simulation reports a change of the tgt population from 40% at 177 °C to 65% at 45 °C. Our result with a 100% of tgt conformation should correspond to the lowest limit of temperature with a maximum number of PEO−water hydrogen bondings.

Concluding Remarks

The adsorption modes of water molecules on the PEO chains predicted by our $V(\boldsymbol{r})$ model and DMol^3 calculations are in good agreement with experimental and computational[19−26] results previously reported in the literature; and suggest that the attractive electrostatic interactions between the positive water O−H bond and the negative minima PEO lone pairs is an important driving force determining the tgt arrangement of the polymer at low concentrations. Adsorption of the water molecules on PEO increases the water minima lone pairs favoring the H_2O−H_2O hydrogen bonds and defining the first hydration shell around the polymer. Inside this shell, water molecules form water−water hydrogen bonds while maintaining the H_2O−PEO hydrogen bonds at the same time. We are in the process of applying theoretical methodologies similar to the ones used in this work in order to analyze the competitive interaction of water and PEO for the Laponite surface in order to provide a more realistic model of the electrostatic interactions present in shake gels. The results will be reported in a future publication.

References and Notes

(1) Harris, J. M. *Poly(Ethylene Glycol) Chemistry: Biotechnical and Biomedical Applications*; Plenum Press: New York, 1992.
(2) Magazu, S. *J. Mol. Struct.* **2000**, *523*, 47.
(3) Choi, H. J.; Kim, C. A.; Sung, J. H.; Kim, C. B.; Chun, W.; Jhon, M. S. *Colloid Polym. Sci.* **2000**, *278*, 701.
(4) Bames, A. C.; Enderby, J. E.; Breen, J.; Leyle, J. C. *Chem. Phys. Lett.* **1987**, *142*, 404.
(5) Bailey, F. E.; Koleske, J. V. In *Ullmann's Encyclopedia of Industrial Chemistry*, Vol. A21; VCH Publishers Inc: New York, 1992.
(6) Devanand, K.; Selser, J. C. *Nature* **1990**, *343* (6260), 739.
(7) Allen, C.; Maysenger, D.; Eisenberg, A. *Colloids Surf., B* **1999,** *16*, 3.
(8) Riley, T.; Godenver, T.; Stolnik, S.; Xiong, C. D.; Garnet, M. C.; Illum, L.; Davis, S. S. *Colloids Surf., B* **1999**, *16*, 147.
(9) Kwon, G. S.; Okano, T. *Adv. Drug Delivery Rev.* **1996**, *21*, 107.
(10) La, S. B.; Okano, T.; *Kataoka*, K. *J. Pharm. Sci.* **1996**, *85*, 85.
(11) Discher, B. M.; Won, Y. Y.; Ege, D. S.; Lee, J. C. M.; Bates, F.; Discher, D. E.; Hammer, D. A. *Science* **1999**, *284*, 1143.
(12) Zabrowski, J.; Prasad, V.; Zhang, W.; Walker, L. M.; Weitz, D. A. *Colloids Surf., A, Phys. Eng. Asp.* **2003**, *123*, 189.
(13) Aray, Y.; Marquez, M.; Rodríguez, J.; Coll, S.; Simón-Manso, Y.; Gonzalez, C.; Weitz, D. A. *J. Phys. Chem. B* **2003**, *107*, 8946.
(14) *Chemical Applications of Atomic and Molecular Electrostatic Potentials*; Politzer, P., Truhlar, D. G., Eds.; Plenum: New York, 1982; Alhambra, C.; Luque, F. J.; Orozco, M. *J. Phys. Chem.* **1995**, *99*, 3084.
(15) *Molecular Electrostatic Potential: Concepts and Applications*; Murray, J. S., Sen, K. D., Eds.; Elsevier: Amsterdam, 1996; Orozco, M.; Luque, F. J. *Theoretical and Computational Chemistry Series*; Murray, J. S., Sen, K., Eds.; Elsevier: Amsterdam, **1996** *3*, 181.
(16) Gadre, S. R.; Shirsat, R. N. *Electrostatics of Atoms and Molecules*: An educational monograph published by the Universities Press: Hyderabad, 2000.
(17) Gadre, S. R.; Babu, K.; Rendell, A. P. *J. Phys. Chem. A* **2000**, *104*, 8976; Leboeuf, M.; Koster, M.; Jug, K.; Salahub, D. R. *J. Chem. Phys.* **1999**, *111*, 4893.
(18) Pingale, S. S.; Gadre, S. R.; Bartoli, L. J. *J. Phys. Chem. A* **1998**, *102*, 9987; Gadre, S. R.; Kulkarni, S. A.; Shivastava, I. A. *J Chem. Phys.* **1992**, *96*, 5253.
(19) Faraone, A.; Magazu, S.; Maisano, G.; Migliardo, P.; Tettamanti, E.; Villari, V. *J. Chem. Phys.* **1999**, *110*, 2.
(20) Bieze, T. W. N.; Barnes, A. C.; Huige, C. J. M.; Enderby, J. E.; Leyle, J. C. *J. Phys. Chem.* **1994**, *98*, 6568.
(21) Devanand, K.; Selser, J. C. *Macromolecules* **1991**, *24*, 5943.
(22) Smith, G. D.; Bedrov, D.; Borodin, O. *Phys. Rev. Lett.* **2000**, *85*, 5583.
(23) Smith, G. D.; Bedrov, D.; Borodin, O. *J. Am. Chem. Soc.* **2000**, *122*, 9548.
(24) Dormidontova, E. E. *Macromolecules* **2002**, *35*, 987.
(25) Bedrov, D.; Smith, G. D. *J. Phys. Chem. B* **1999**, *103*, 3791.
(26) Bedrov, D.; Pekny, M.; Smith, G. D. *J. Phys. Chem. B* **1998**, *102*, 996.
(27) Wade, L. G., Jr. *Organic Chemistry*; Prentice Hall, Inc.: New York, 1987; Pophristic, V.; Goodman, L. *Nature* **2001**, *411*, 565.
(28) Del Bene, J. E.; Szczepaniak, W. B. *J. Phys. Chem.* **1995**, *99*, 10705; Adamo, C.; Barone, V. In *Recent Advances in Density Functional Methods*, Part II; Chong, P. Delano, Ed.; World Scientific: Singapore, 1997.
(29) Keith, T. A.; Bader, R. F. W.; Aray, Y. *Int. J. Quantum Chem.* **1996**, *183*, 183.
(30) DMol^3 is available as part of Material Studio., Accelrys Inc., San Diego, CA, 2002.
(31) Delley, B. *J. Chem. Phys.* **1990**, *92*, 508; Delley, B. *J. Chem. Phys.* **2000**, *113*, 7756.
(32) Perdew, J. P.; Burke, K.; Emzerhof, M. *Phys. Rev. Lett.* **1996**, *77*, 3865.
(33) Aray, Y.; Rodriguez, J.; Lopez-Boada, R. *J. Phys. Chem.* **1997**, *101*, 2178.
(34) Aray, Y.; Rodriguez, J.; Vega, D. *Comput. Phys. Commun.* **2002**, *143*, 199.
(35) *Numerical Recipes in Fortran 77: The Art of Scientific Computing*; Cambridge University Press: New York, 1992; p 708.
(36) www.accelrys.com/mstudio/ms_modeling/amorphous.html
(37) www.accelrys.com/references/dmol3.html; and Hamann, D. R.; Schluter, M.; Chaing, C. *Phys. Rev. Lett.* **1979**, *43*, 1494.